An Empirically Optimized One-Electron Pseudopotential for the Hydrated Electron. A Proof-of-Concept Study

Pauf Neupane, † David M. Bartels, *,‡ and Ward H. Thompson*,†

†Department of Chemistry, University of Kansas, Lawrence, KS 66045, USA ‡Radiation Laboratory, University of Notre Dame, Notre Dame, Indiana 46556, United States

E-mail: bartels.5@nd.edu; wthompson@ku.edu

September 13, 2023

Abstract

Mixed quantum-classical molecular dynamics simulations have been an important tool for studying the hydrated electron. They generally use a one-electron pseudopotential to describe the interactions of the electron with the water molecules. This approximation is both the strength and weakness of the approach. On the one hand, it enables extensive statistical sampling and large system sizes that are not possible with more accurate ab initio molecular dynamics methods. On the other hand, there has (justifiably) been much debate about the ability of pseudopotentials to accurately and quantitatively describe the hydrated electron properties. These pseudopotentials have largely been derived by fitting to ab initio calculations of an electron interacting with a single water molecule. In this Paper, we present a proofof-concept demonstration of an alternative approach in which the pseudopotential parameters are determined by optimizing them to reproduce key experimental properties. Specifically, we develop a new pseudopotential, using the existing TBOpt model as a starting point, which correctly describes the hydrated electron vertical detachment energy and radius of gyration. In addition to these properties, this

empirically optimized model displays a significantly modified solvation structure, which improves, for example, the prediction of the partial molar volume.

1 Introduction

The hydrated electron (e_{aq}^-) is an exotic and unique chemical species that lacks a nucleus and whose behavior has been the focus of controversy for more than five decades. Owing to its fundamental importance in radiation chemistry, 1-5 photochemistry, 6,7 electrochemistry, and theoretical chemistry, 4,9,10 determined efforts have been expended in the pursuit of an accurate molecular-level description of the hydrated electron. 11-19 To this day many questions remain unanswered about excess electrons in water that range from basic aspects of its structure (vide infra) to the mechanisms of its reactions. 20

Efforts to address these issues *via* theoretical modeling of the hydrated electron has largely proceeded along two tracks. The first makes use of a one-electron pseudopotential that represents the effective interactions of the excess electron with the water molecules. ^{11–14,21–25} The electron is then described quantum mechanically, either using path integrals ^{21,23,26,27} or adiabatic solution of the Schrödinger equation, ^{12–14,25,28,29} The second exploits recent ad-

vances in both methodology and computing power to use density functional theory (DFT), or other electronic structure-based, modeling of the excess electron in liquid water. ^{15–17,19,30–32} As we now discuss, each approach has its own advantages (and disadvantages) that make it useful (but also limited) in investigations of the hydrated electron.

A thorough discussion of the development and application of pseudopotentials for the hydrated electron up to roughly a decade ago has been presented by Turi and Rossky, 10 and we refer the reader to that review. Most relevant to the present work are the more recent efforts to test the predictions of different pseudopotentials against a wide range of measured hydrated electron properties. 9,25,33-41 Many of these were motivated by arguments over whether the excess electron possesses a cavity or a noncavity structure in water. 9,13,42-44 The argument now appears settled in favor of a cavity structure, ^{19,39,44,45} but this flurry of validation work has both spurred the development of new pseudopotentials²⁵ and revealed a number of strengths and weaknesses of extant ones.

Indeed, DFT-based simulations are consistent with a cavity-forming picture of the electron, but otherwise reveal some stark differences with the pseudopotential descriptions that predict the same basic structure. This is most evident in the electron-water radial distribution function (RDF), which characterizes the electron's solvation environment and is significantly more structured in the DFT descriptions. For example, the height of the first solvation shell peak from simulations using different pseudopotentials ^{12–14,25–27} ranges from 1.1 to 1.7 while different DFT-based treatments 15-17,19,32 give heights of 1.7-3.5. The large spread in the DFT results are likely indicative of a lack of convergence, potentially related to any or all of the system size, statistical sampling, or density functional; these issues have been recently pointed out by Park and Schwartz. 19 However, the improved description of the excess electron interactions with multiple water molecules, compared to that of pseudopotentials, provides strong motivation for DFT studies. Nevertheless, it is certainly the case that the computational expense of DFT descriptions of the hydrated electron will continue to limit the feasible system sizes and trajectory lengths for at least the near future, though neural network-based potentials show some promise for improving this situation. ^{18,46} This means one-electron pseudopotentials will continue to have an important role in elucidating solvated electron properties as they enable simulations of large systems, propagation of long trajectories that provide significant statistical sampling, and ready analysis for physical insight.

Advancement in the ability of pseudopotentials to faithfully reproduce the characteristics of the hydrated electron is needed. ^{25,41,44,47} This is apparent from comparisons to both measured properties and electronic structurederived pictures of the solvation structure as noted above. These shortcomings of currently available one-electron pseudopotentials motivate new approaches to developing such models for the hydrated electron.

In this Paper, we propose one such method based on optimization of the pseudopotential parameters to match empirical data. We choose the average vertical detachment energy and radius of gyration as the two target properties because they have been accurately determined experimentally $^{48-52}$ and also provide some tension within the description, *i.e.*, pseudopotentials can accurately predict one of these properties but often not both. 25,40 The present proof-of-concept study demonstrates that this approach can yield an improved pseudopotential, including with respect to properties that are not directly optimized.

2 Methodology

2.1 Pseudopotential Optimization

In this work, we use an empirical mapping method to optimize the pseudopotential parameters for hydrated electron interaction with the classical water in the mixed quantum classical molecular dynamics (QC-MD) simulation. Specifically, we use the gradient descent method

to minimize the score function S, defined as

$$S(\vec{\alpha}) = \sum_{i} \frac{w_i \left[\langle f_i(\vec{\alpha}) \rangle - f_{i,expt.} \right]^2}{f_{i,expt.}^2}, \quad (1)$$

where $\vec{\alpha} = (\alpha_1, \alpha_2, \dots, \alpha_M)$ is the set of pseudopotential parameters to be optimized, $\langle f_i(\vec{\alpha}) \rangle$ is the calculated average value of property f_i with corresponding measured value $f_{i,expt}$, and w_i is the weight in the score function for the i^{th} property. In this proof-of-concept study we consider just two key properties of the hydrated electron: 1) The radius of gyration R_g that measures the size of the electron cloud, and 2) The vertical detachment energy VDE, that characterizes its binding energy to the liquid.

In the gradient descent method, the parameters $\vec{\alpha}$ are optimized by minimizing the score function. In each iteration, the gradient of the score function with the current parameters, $\vec{\alpha}_n$, is calculated in QC-MD simulations and the new parameters, $\vec{\alpha}_{n+1}$, are obtained by following this gradient:

$$\vec{\alpha}_{n+1} = \vec{\alpha}_n - \gamma_n \vec{\nabla}_\alpha S(\vec{\alpha}_n). \tag{2}$$

Note that, in this work, $f_1 = R_g$ and $f_2 = VDE$. We find that the VDE is significantly more sensitive than R_g to the changes in the pseudopotential parameters. Hence we assigned $w_1 = 10$ for R_g and $w_2 = 1$ for the VDE. Preliminary tests indicated that equal weights do not readily lead to convergence for the average R_g value and other, smaller, values for w_1 lead to slower convergence. The step size for the n^{th} iteration is given by

$$\gamma_n = \frac{|(\vec{\alpha}_n - \vec{\alpha}_{n-1})^T \cdot [\vec{\nabla}S(\vec{\alpha}_n) - \vec{\nabla}S(\vec{\alpha}_{n-1})]|}{|\vec{\nabla}S(\vec{\alpha}_n) - \vec{\nabla}S(\vec{\alpha}_{n-1})|^2},$$
(3)

which relies on the gradient for the previous iteration.

To compute $\nabla S(\vec{\alpha}_n)$ from eq. 1, we need the derivative of average properties w.r.t. the parameters α_j . Each property, f_i , of the hydrated electron can be related to a thermal average of

an expectation value over QC-MD trajectories:

$$\langle f_i(\vec{\alpha}) \rangle = \frac{1}{Q} \int dp \int dq \, e^{-\beta H} \langle \psi_0 | \hat{f}_i(\vec{\alpha}) | \psi_0 \rangle$$
$$= \frac{1}{Q} \text{Tr} \left[e^{-\beta H} \langle \psi_0 | \hat{f}_i(\vec{\alpha}) | \psi_0 \rangle \right]. \tag{4}$$

Here, Q is the canonical partition function, $\beta = 1/k_BT$ with k_B Boltzmann's constant and T the temperature, and H is the classical adiabatic Hamiltonian of the system, and ψ_0 is the ground-state hydrated electron wave function. It is important to note that Q, H, and ψ_0 all also depend on the pseudopotential parameters $\vec{\alpha}$. In the following we use Tr to represent the phase space integrals. Then the partial derivative of eq. 4 with respect to a particular parameter, α_i , is given by

$$\frac{\partial \langle f_i \rangle}{\partial \alpha_j} = -\frac{1}{Q^2} \frac{\partial Q}{\partial \alpha_j} Tr \left[e^{-\beta H} \langle \psi_0 | \hat{f}_i | \psi_0 \rangle \right]
- \frac{\beta}{Q} Tr \left[e^{-\beta H} \frac{\partial V}{\partial \alpha_j} \langle \psi_0 | \hat{f}_i | \psi_0 \rangle \right]
+ \frac{1}{Q} Tr \left[e^{-\beta H} \frac{\partial}{\partial \alpha_i} \langle \psi_0 | \hat{f}_i | \psi_0 \rangle \right]. (5)$$

In other words, there are contributions from the partition function, the Boltzmann factor, and the property expectation value.

Noting that $Q = Tr[e^{-\beta H}]$, it is straight forward to show that

$$\frac{\partial \langle f_i \rangle}{\partial \alpha_j} = -\beta \left\langle \delta \left(\frac{\partial V}{\partial \alpha_j} \right) f_i \right\rangle
+ \frac{1}{Q} Tr \left[e^{-\beta H} \frac{\partial}{\partial \alpha_i} \langle \psi_0 | \hat{f}_i | \psi_0 \rangle \right], (6)$$

where $\delta(\partial V/\partial \alpha_j) = \partial V/\partial \alpha_j - \langle \partial V/\partial \alpha_j \rangle$ is the fluctuation in potential energy derivative.

It remains then to determine the derivatives of the expectation values corresponding to R_g and VDE. The latter is more straightforward and we consider it first. The VDE is equal to the negative of the ground-state electron energy, such that $f_i = -E_0$ and therefore $\hat{f}_i = -\hat{h}_{el}$. Here, Thus \hat{h}_{el} is the quantum mechanical Hamiltonian for the electron and can be written as $\hat{h}_{el} = \hat{T}_{e^--w} + \hat{V}_{e^--w}$. However, only the second, potential energy contribution

that comes from the pseudopotential depends on $\vec{\alpha}$. Thus, we have

$$\frac{\partial}{\partial \alpha_{j}} \langle \psi_{0} | \hat{h}_{el} | \psi_{0} \rangle = \left\langle \psi_{0} \left| \frac{\partial \hat{h}_{el}}{\partial \alpha_{j}} \right| \psi_{0} \right\rangle
= \left\langle \psi_{0} \left| \frac{\partial \hat{V}_{e^{-}-w}}{\partial \alpha_{j}} \right| \psi_{0} \right\rangle
= \frac{\partial V}{\partial \alpha_{j}}.$$
(7)

This result makes use of the Hellmann-Feynman theorem,⁵³ and also notes that the full classical potential energy, V, is composed of the water-water interactions that are independent of $\vec{\alpha}$ plus the expectation value of the electron-water potential, $\langle \psi_0 | \hat{V}_{e^--w} | \psi_0 \rangle$. Thus, for the derivative of the average VDE we obtain

$$\frac{\partial \langle VDE \rangle}{\partial \alpha_j} = -\beta \left\langle \delta \left(\frac{\partial V}{\partial \alpha_j} \right) VDE \right\rangle
- \left\langle \frac{\partial V}{\partial \alpha_j} \right\rangle,$$
(8)

which can be straightforwardly calculated within QC-MD simulations.

To obtain the derivative when $f_i = R_g$, we first evaluate the derivative for $\hat{f}_i = \hat{R}_g^2 = (\hat{\vec{r}} - \langle \hat{\vec{r}} \rangle_0)^2$ and use

$$\frac{\partial \langle R_g \rangle}{\partial \alpha_j} = \frac{1}{2\langle R_g \rangle} \frac{\partial \langle R_g^2 \rangle}{\partial \alpha_j}.$$
 (9)

Here, $\hat{\vec{r}}$ is the coordinate operator for the electron and $\langle \hat{\vec{r}} \rangle_0$ is its ground-state expectation value, *i.e.*, average position.

For this squared radius of gyration, eq. 6 becomes

$$\frac{\partial \langle R_g^2 \rangle}{\partial \alpha_j} = -\beta \left\langle \delta \left(\frac{\partial V}{\partial \alpha_j} \right) R_g^2 \right\rangle$$

$$+ \frac{1}{Q} Tr \left[e^{-\beta H} \frac{\partial}{\partial \alpha_j} \langle \psi_0 | (\hat{\vec{r}} - \langle \hat{\vec{r}} \rangle_0)^2 | \psi_0 \rangle \right],$$

Unlike in the case of the VDE, the second term cannot be evaluated using the Hellmann-Feynman theorem and is instead calculated using the general formula derived by Aizu:⁵⁴

$$\frac{\partial \langle \psi_0 | \hat{A} | \psi_0 \rangle}{\partial \alpha_j} = \sum_{i \neq 0} \frac{\langle \psi_0 | \frac{\partial \hat{h}_{el}}{\partial \alpha_j} | \psi_i \rangle \langle \psi_i | \hat{A} | \psi_0 \rangle + \langle \psi_0 | \hat{A} | \psi_i \rangle \langle \psi_i | \frac{\partial \hat{h}_{el}}{\partial \alpha_j} | \psi_0 \rangle}{E_0 - E_i} + \langle \psi_0 | \frac{\partial \hat{A}}{\partial \alpha} | \psi_0 \rangle, \tag{11}$$

For $\hat{A} = (\hat{\vec{r}} - \langle \hat{\vec{r}} \rangle_0)^2$, the last term vanishes because the electron coordinate is independent of

the pseudopotential parameters. Thus, we have

$$\frac{\partial \langle \psi_0 | (\hat{\vec{r}} - \langle \hat{\vec{r}} \rangle_0)^2 | \psi_0 \rangle}{\partial \alpha_j} = 2 \sum_{i \neq 0} \frac{\langle \psi_0 | \frac{\partial \hat{V}_{e^- - w}}{\partial \alpha_j} | \psi_i \rangle \langle \psi_i | (\hat{\vec{r}} - \langle \hat{\vec{r}} \rangle_0)^2 | \psi_0 \rangle}{E_0 - E_i}, \tag{12}$$

$$\frac{\partial \langle R_g^2 \rangle}{\partial \alpha_j} = -\beta \left\langle \delta \left(\frac{\partial V}{\partial \alpha_j} \right) R_g^2 \right\rangle + 2 \left\langle \sum_{i \neq 0} \frac{\langle \psi_0 | \frac{\partial \hat{V}_{e^- - w}}{\partial \alpha_j} | \psi_i \rangle \langle \psi_i | (\hat{\vec{r}} - \langle \hat{\vec{r}} \rangle_0)^2 | \psi_0 \rangle}{E_0 - E_i} \right\rangle (13)$$

Note that this requires, in the second term, a sum over excited states of the hydrated electron, which makes the derivative calculation more expensive than that for the VDE. In practice, we find this sum is converged using five excited states.

To calculate the derivatives of the average R_g and VDE, the derivatives of the e^- -water pseudopotential are needed. We consider as the functional form for optimization the TB pseudopotential created by Turi and Borgis¹² and modified by Glover and Schwartz²⁵ to generate the TBOpt model (also known as TBSE+OptPol). The form of these pseudopotentials is the sum of an excess electron interaction potential V_x for oxygen (ox) and hydrogen (hy) sites on water molecules,

$$V(r_x) = -\frac{q_x}{r_x} \operatorname{erf}(A_{1,x} r_x)$$

$$+ \frac{B_{1,x}}{r_x} \left[\operatorname{erf}(B_{2,x} r_x) - \operatorname{erf}(B_{3,x} r_x) \right],$$
(14)

and a polarization potential V_{pol} ,

$$V_{pol}(r_{ox}) = -\frac{\alpha_w}{2(r_{ox}^2 + C_{1,ox}^2)^2}.$$
 (15)

Here, x refers to ox or hy and q_x and r_x are the respective site charge and electron-x site distance. Finally, α_w is the water polarizability parameter.

The TBOpt pseudopotential differs from the TB one only in the two polarization potential parameters, α_w and $C_{1,ox}$, and has been shown to predict the hydrated electron properties in better agreement with experiment.²⁵ In the present work we consider nine pseudopotential parameters, $\vec{\alpha}$ = $(A_{1,ox}, B_{1-3,ox}, A_{1,hy}, B_{1-3,hy}, C_{1,ox})$. We use the TBOpt parameters as the initial potential for the optimization. We used the same approach with the TB pseudopotential as the starting point, but were unable to significantly improve the radius of gyration. This points to a particular sensitivity of the hydrated electron on the water polarizability value, α_w , which is the only non-adjusted parameter that differs between the two models. This suggests that including α_w as an adjustable parameter may be fruitful and we plan to investigate this in future work.

2.2 Simulation Details

To optimize the pseudopotential parameters, we performed QC-MD simulations of 500 water molecules and one excess electron in a cubic box of side length 24.663603 Å. We model water with the SPC/Fw force field.⁵⁵ This water model has the same charges as, but a simpler intramolecular potential than, the SPC/Flexible⁵⁶ water model that is commonly used in hydrated electron studies; we have previously shown that it gives similar behavior for the hydrated electron.²⁰ The simulations are performed in a cannonical (NVT)ensemble with periodic boundaries in all directions. Initial velocities are assigned randomly at 298.15 K, drawn from the Boltzmann distribution. The classical equations of motion are integrated with the velocity Verlet algorithm using a time step of 1 fs. Temperature is maintained at 298.15 K using a Bussi-Donadio-Parrinello thermostat.⁵⁷ The Lennard-Jones interactions are truncated at 10 Å. The electrostatic interactions were also truncated at 10 Å; no effect of long-range electrostatics was included in this proof-of-concept study.

For the quantum mechanical calculation of the adiabatic electron wavefunction at each time step in the QC-MD simulation, the Schrödinger equation is solved using a sincfunction discrete variable representation (DVR) basis. 58 The DVR basis spans from -7 to 6.125 Å with $16 \times 16 \times 16$ grids (grid spacing 0.875 Å). The eigenvalue equation is solved using an iterative Lanczos algorithm with full reorthogonalization.

At each iteration of the pseudopotential optimization we propagated a set of 20 trajectories for 13 ps each. The last 10 ps from each run, yielding a total of 200 ps simulation time, is used for computing the derivatives in Eqs. 8 and 13. The optimized parameters are then used to simulate the excess electron with 1372 water molecules in an NpT ensemble using a Bernetti-Bussi barostat, ⁵⁹ and the details of the simulations are as just described except we propagated 5 sets of the trajectories for better averaging. The error bars are reported as 95% confidence intervals based on the Student's t-distribution ⁶⁰

3 Results and Discussion

3.1 Pseudopotential Optimization

We first performed simulations with the TBOpt pseudopotential (iteration 0). The simulation runs from each iteration were used to generate the new pseudopotential parameters for the next iteration using the method explained in Sec. 2.1 that involves computation of the derivatives of the average properties. The step size γ is determined from two successive iterations, so for the first iteration, we manually choose $\gamma = 0.1$ such that the resulting parameters produces significant shift in R_g and VDE towards the experimental results.

The TBOpt pseudopotential with SPC/Fw water (and no long-range electrostatics) is found to overestimate the VDE and underestimate the R_g , as shown in Fig. 1. We find $\langle VDE \rangle = 4.46$ eV, and $\langle R_g \rangle = 2.25$ Å, compared to the experimental values 9,49 of 3.77 eV and 2.45 Å, respectively. In developing the TBOpt model, Glover and Schwartz found good agreement of these properties with experimental results ($\langle VDE \rangle = 3.62$ eV and $\langle R_g \rangle = 2.48$ Å). We are unsure of the origin of these differences. They could be attributable to the difference in water models, but we have previously found much weaker dependences on the water model. 20,41

As we optimize the pseudopotential parameters, we find that $\langle R_g \rangle$ increases monotonically toward the experimental value. This convergence is shown in Fig. 2 and the R_g distributions for the even-numbered iterations are plotted in Fig. 1a. The VDE, which is overall more sensitive to the pseudopotential details (as reflected in the difference in weights in the score function, eq. 1), exhibits a non-monotonic convergence, but is consistently within 0.2 eV of the target value after the first iteration. This can be seen in Fig. 2 where the score function is also plotted. We find a rapid initial drop in

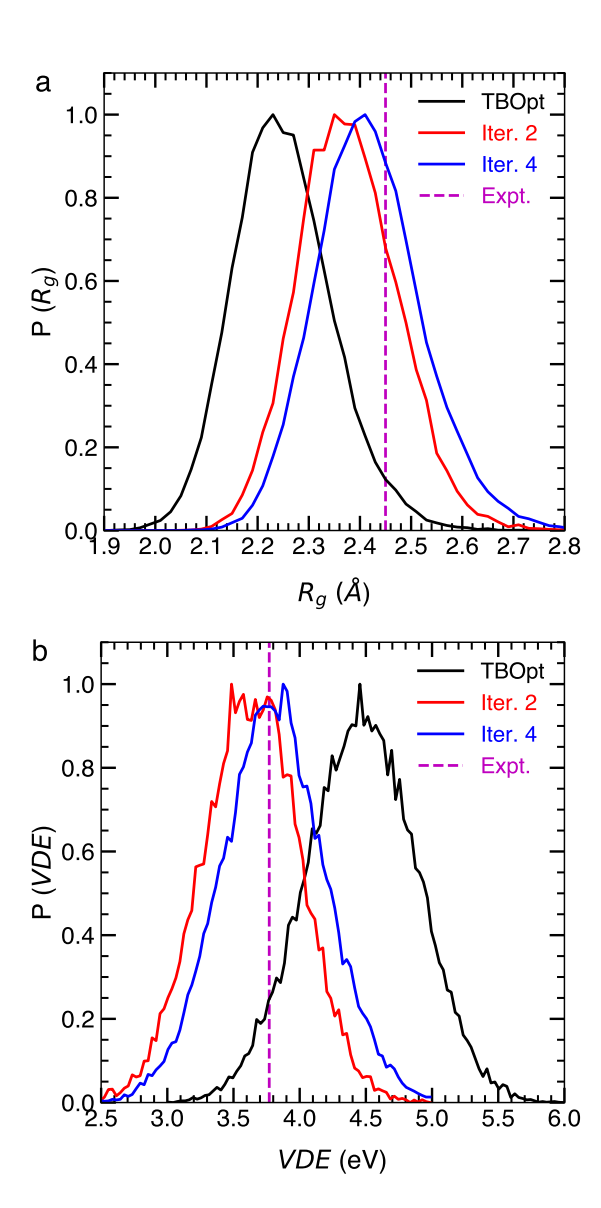


Figure 1: The a) R_g and b) VDE distributions (solid lines) are shown for different iterations in the optimization. The mean values of the distributions are converging toward the experimental values shown as dashed lines.

S in the first iteration, arising from the change in the $\langle VDE \rangle$ followed by a slow decay associated with the increasing value of $\langle R_g \rangle$. For iteration 4 and 5, both the vertical detachment energy and radius of gyration are quite close to the target values (S < 0.05); we choose the results of iteration 4 as our optimized set as they have a slightly lower score function value. These parameters for the empirically optimized pseudopotential, which we denote henceforth as the EOP23 model, are given in Table 1 along with the original TBOpt values.

Table 1: Parameters for EOP23 and TBOpt²⁵ pseudopotentials in atomic units.

Parameter	EOP23		TBOpt	
	OX	hy	OX	hy
$\overline{\mathbf{A}_{1,x}}$	0.549	0.731	0.575	0.750
$\mathrm{B}_{1,x}$	0.620	0.151	0.620	0.150
$\mathrm{B}_{2,x}$	0.995	0.523	1.000	0.500
$\mathrm{B}_{3,x}$	0.429	0.284	0.400	0.350
$C_{1,x}$	1.973		2.07	

It is interesting to examine the evolution of the R_g and VDE distributions during the optimization in Fig. 1. In particular, we find that the widths of the distributions do not change significantly as the centers shift toward the target values. These VDE distributions show the non-monotonic behavior observed in Fig. 2, where the iteration 2 distribution is shifted to values that are too low relative to the experimental target.

The behavior is different for the hydrated electron solvation structure, which qualitatively changes during the optimization, as shown by the electron-hydrogen and electronwater center-of-mass radial distribution functions (RDFs) plotted in Fig. 3. For the electron-hydrogen RDF, Fig. 3a, the optimization does not change the longer-range, r > 4 Å, behavior, but the behavior at shorter distances is strongly modified. In particular, the EOP23 result (labeled Iteration 4 in the figure) shows a significantly reduced first-solvation shell peak, a second solvation shell peak at larger distances, a lower minimum between the two shells, and a

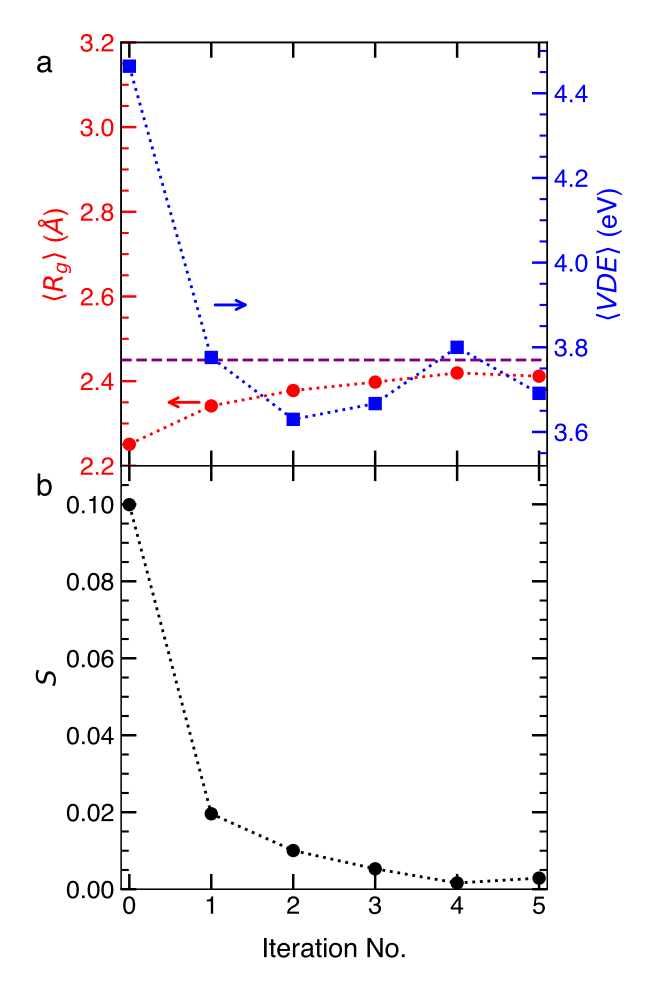


Figure 2: (a) The $\langle R_g \rangle$ (red) and $\langle VDE \rangle$ (blue) of hydrated electron, and (b) score function value S shown for the even-numberred iterations in the optimization. The markers (squares and circles) represent data and the dotted lines are shown to guide the eye. The dashed line shows experimental result for $\langle R_g \rangle$ (left axis) and $\langle VDE \rangle$ (right axis).

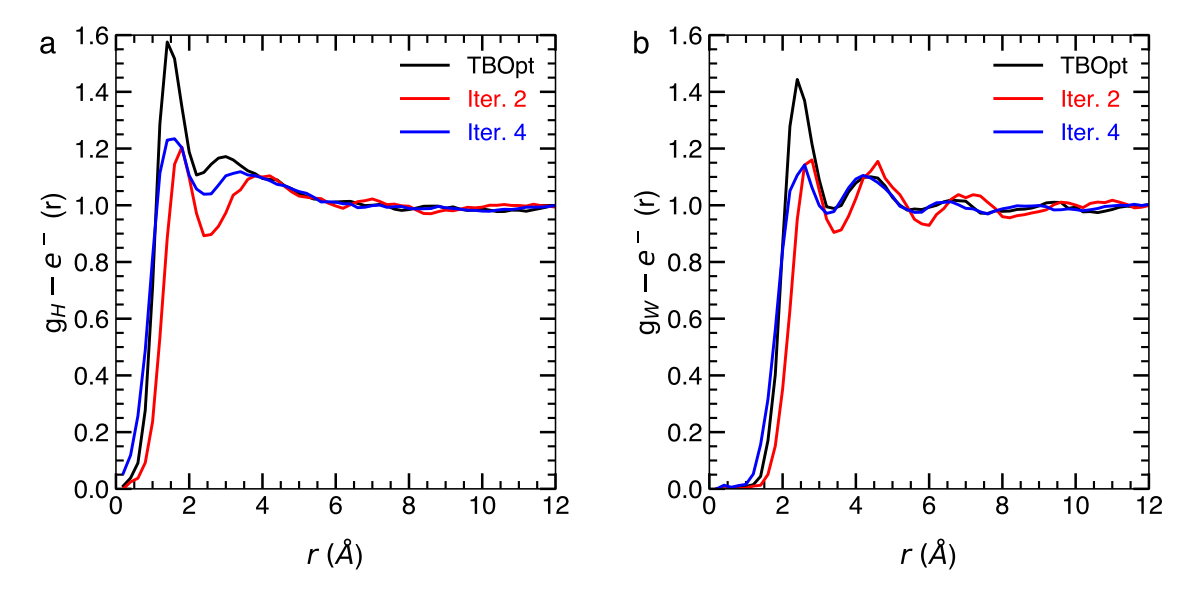


Figure 3: The RDF, g(r), for a) e⁻-water H atom and b) e⁻-water center-of-mass for the even-numbered iterations of the optimization.

closer approach to the center of the electron distribution. In general, these suggest more oriented water molecules solvating the hydrated electron.

In the case of the electron-water center-of mass shown in Fig. 3b, the TBOpt pseudopotential yields an RDF with a larger first solvation shell peak followed by decreasing peak heights for the second and third solvation shells; the minima between the solvation shell peaks fall only to near one. In contrast, as the optimization proceeds, the first solvation shell peak decreases significantly in intensity so that it lies at nearly the same level as the second peak. Moreover, the RDF drops below one between the solvation shells, which is an important property with respect to the partial molar volume. 41 We will discuss these properties of EOP23 model in more detail in Sec. 3.3. Finally we note that at small r, the EOP23 RDF shows a non-zero feature associated with rare occasions where a water molecule briefly lies within the hydrated electron cavity. This suggests that the optimization has added increased the fluxionality of the hydrated electron structure.

3.2 EOP23 Pseudopotential Properties

We next consider the effect of the empirical optimization on the electron interactions with a single water molecule. This is instructive because pseudopotentials are typically parameterized based on electronic structure calculations of this minimal system.

The TBOpt pseudopotential differs from the original TB form only in the polarization term in eq. 15, which we consider first. Specifically, Glover and Schwartz reduced the rigidity of the potential by reducing the water polarizability, α_w , and the $C_{1,ox}$ parameter. ²⁵ In the empirical optimization presented here, we fixed the polarizability at the TBOpt value, but include $C_{1,ox}$ in the set of parameters that are optimized. The optimization results in further reduction of the $C_{1,ox}$ parameter (see Table 1), resulting in a more attractive electron interactions with the water molecule at short distances. This is shown in Fig. 4, where the polarization potential V_{pol} is plotted as a function of distance from the oxygen atom with the oxygen located at the origin.

We also examine the behavior of the full pseudopotential along several directions through a water molecule. These are shown in Fig. 5 where they are compared to the TB and TBOpt

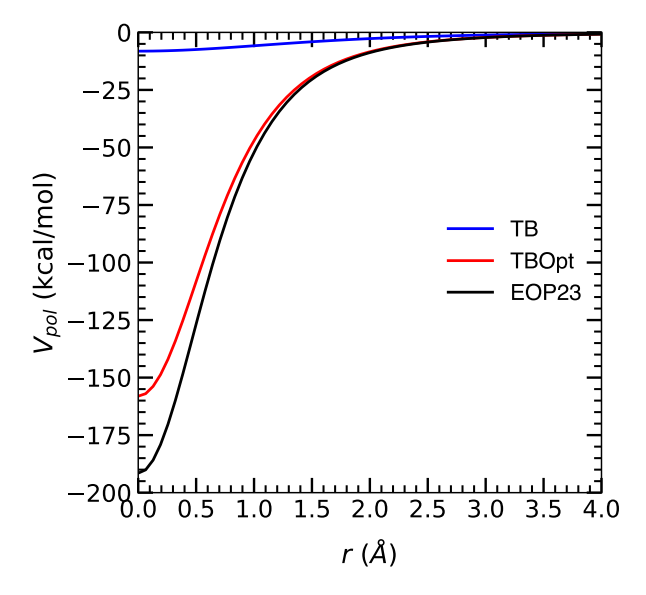


Figure 4: The empirically optimized, EOP23 (black line), polarization potential V_{pol} , eq. 15, as a function of electron-oxygen atom distance is compared to that for the TB (blue line) and TBOpt (red line) pseudopotentials.

models. The clear conclusion from these energy profiles is that the optimization has two primary effects. First, it makes the pseudopotential significantly less repulsive around the oxygen atom, as can be seen from the height of the peak near r=0 in each plot. Second, it makes the potential somewhat less attractive around the hydrogen atoms compared to the TBOpt model, while still keeping it more attractive than the TB potential. This effect can be seen in all three slices through the potential, but is most clearly evident in Fig. 5c. We expect that the second effect is the more important one for the hydrated electron properties given that the potential around the oxygen atom remains strongly repulsive and likely has more minor effects on the electron density in that region.

3.3 The Hydrated Electron within the EOP23 Pseudopotential

With the optimized, EOP23, pseudopotential parameters in hand, we ran further simulations to better characterize the properties of the hydrated electron. In particular, we aimed to probe two key properties that were not explicitly part of the empirical optimization proce-

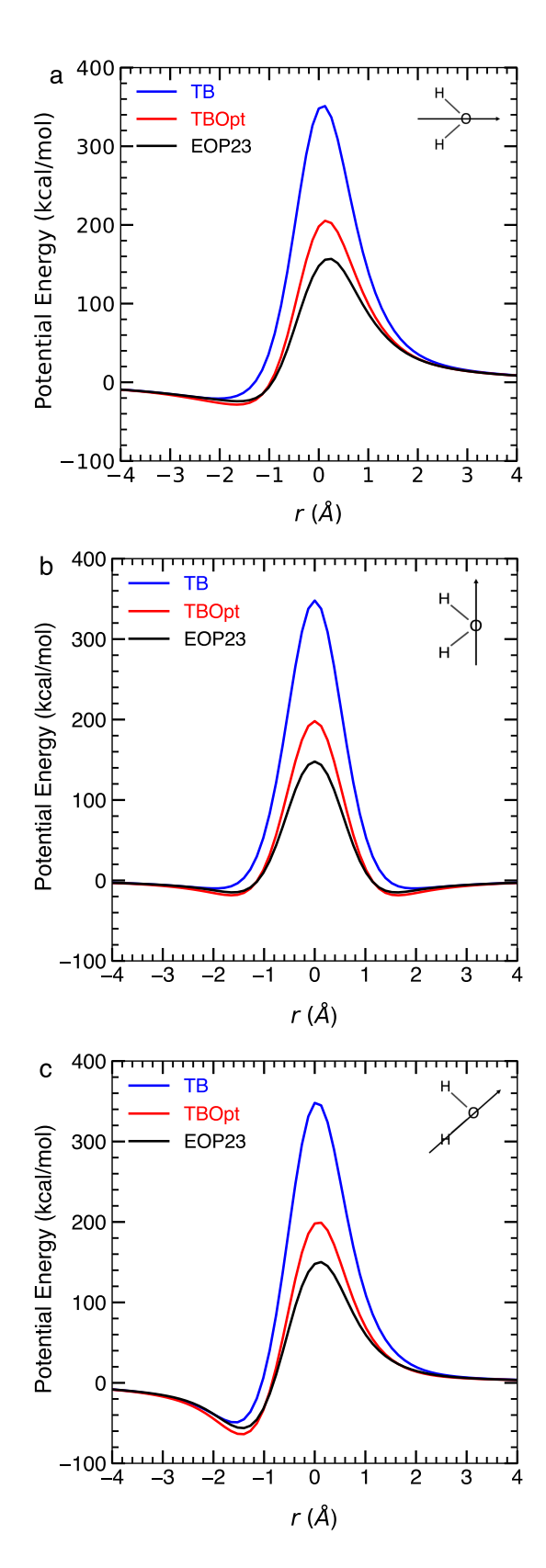


Figure 5: Total pseudopotential energy for an excess electron interacting with a single water molecule along a) the bisecting, dipole direction (x-axis), b) an in-plane axis perpendicular to the water dipole (y-axis, with the molecule in the xy-plane), and c) the OH bond axis.

dure: The partial molar volume and the temperature dependence of the optical spectrum. The former is properly calculated at constant pressure and the latter has been measured at constant pressure. Thus, we propagated five (three) sets of NpT trajectories at 1 atm and 298.15 K (all other T), with each set composed of twenty 13 ps independent trajectories with the first 3 ps (5 ps) discarded as equilibration for 298.15 K (all other T). This yields 1.0 nstotal simulation time at 298.15 K, and 0.48 ns at all other T, for data analysis. We also simulated a set of trajectories with TBOpt pseudopotential for comparison. These NpT simulations are performed for a larger system of 1372 water and one excess electron, which is required for the partial molar volume, V_M calculation ⁴¹ using the Kirkwood-Buff (KB) method. 61–63

We first examine the e^- -water radial distribution function, which is shown in Fig. 6a. It shows a cavity of radius ~ 2 Å (measured by where the RDF first reaches a value of 1). This is similar to that for the TBOpt model, but smaller than the cavity for the original Turi-Borgis pseudopotential. 12 As noted above, the largest result of the optimization is a reduction in the height of the first solvation shell peak. In the EOP23 model it reaches a maximum of 1.2 at r=2.6 Å, compared to a height of 1.4 for the TBOpt case. The coordination number, obtained from the first solvation shell is 5.2 compared to 5.8 for the TBOpt model.

This RDF can be used to obtain the partial molar volume using the approach of Kirkwood and Buff. $^{61-63}$ We have recently estimated V_M for some of the widely used pseudopotentials, including TBOpt, 41 using this method, which gives the partial molar volume as

$$V_M = k_B T \kappa_T - G_{e^--wat}, \tag{16}$$

where κ_T is the isothermal compressibility of the water solvent and

$$G_{e^--wat} = \int_0^R [g_{e^--wat}(r) - 1] w(r; R) dr, (17)$$

is the KB integral determined from the electron-water center-of-mass RDF. Here, $w(r;R) = 4\pi r^2 [1 - (3x/2) + (x^3/2)]$ is a weight-

ing function that corrects for finite-size effects. $^{63-65}$

The running partial molar volume (i.e., eq. 17) as a function of R) obtained with the EOP23 pseudopotential is shown in Fig. 6b, where it is compared with analogous results for TBOpt. A key caveat necessary for interpreting these results is that we have not included the long-range electrostatic interactions in the present work; these serve to densify the water, which significantly changes the magnitude of V_M (making comparisons with experiment inappropriate), though not the trends in comparing the two pseudopotentials. We find that the EOP23 pseudopotential yields a partial molar volume of $+16 \pm 2$ cm³/mol compared to $+11 \pm$ 1 cm³/mol for the TBOpt model. Note that we previously found $V_M = -15 \pm 4 \text{ cm}^3/\text{mol for}$ TBOpt when using an Ewald sum for describing long-range electrostatic effects, 20 which is qualitatively at odds with the measured value of $26\pm6~\mathrm{cm^3/mol.}^{45,66}$ When an Ewald sum is used with the EOP23 pseudopotential, we obtain $V_M = -7 \text{ cm}^3/\text{mol}$ (see the Supporting Information). Thus, the key point of the present calculations are that the optimized EOP23 pseudopotential shifts the partial molar volume in the correct direction, though the change is not of sufficient magnitude to generate agreement with the experimental V_M .

Another key aspect of the hydrated electron pseudopotential descriptions that has received significant attention is the temperature dependence of the properties. Thus, we have examined how the radius of gyration and vertical detachment energy vary with temperature at constant pressure. These results are shown in Fig. 7 for temperatures from 280 to 370 K. Note that the different density of the NpT simulations results in a slightly larger average VDE at room temperature compared to the NVT conditions of the optimization simulations, though the room temperature R_q distribution is little affected. We find that the EOP23 pseudopotential predicts that $\langle R_q \rangle$ grows with increasing temperature. This arises from a shift in the, already asymmetric, R_q distribution with increasing T, which is particularly apparent on the high R_q side. This result is consistent with

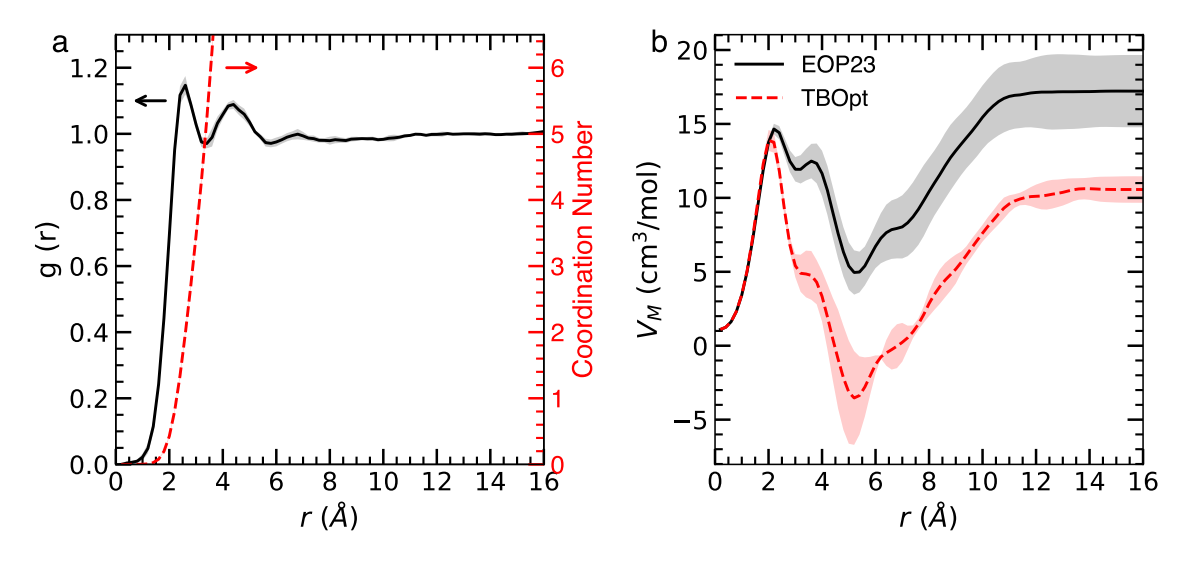


Figure 6: a) The e^- -water radial distribution function (solid line) and running coordination number (dashed line), and b) the running partial molar volume of the hydrated electron. The shaded regions indicate 95% confidence limits.

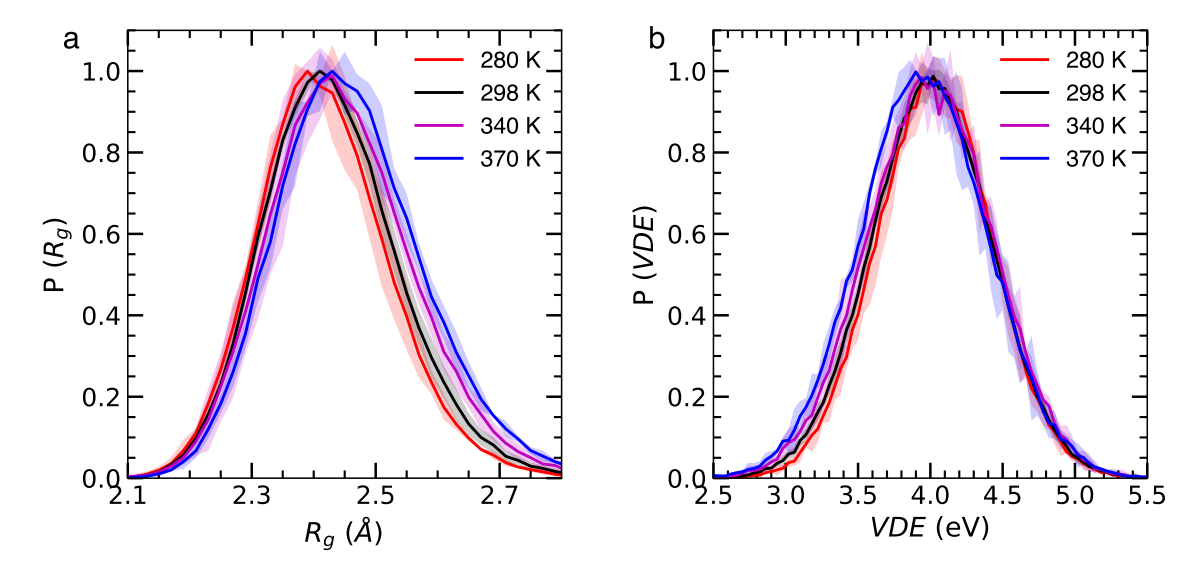


Figure 7: The distribution of the a) radius of gyration (R_g) and b) vertical detachment energy (VDE) for the EOP23 pseudopotential at four different temperatures. The shaded regions indicate 95% confidence limits.

the ab initio-derived machine learning potential simulations by Lan et al. at 250 bar, who observed an increase in $\langle R_g \rangle$ with $T.^{46}$ We see a weaker temperature dependence in the average vertical detachment energy. The VDE distribution, Fig. 7b only modestly shifts the peak position with T and the primary effect is a slight broadening of the distribution on the low VDE side. This is generally consistent with the results of Ref. 46 that $\langle VDE \rangle$ decreases with increasing temperature at 250 bar; they observe a decrease from 300 to 373 K of \sim 0.09 eV compared to \sim 0.06 eV with EOP23.

Another salient feature of the hydrated electron is the temperature dependence of its optical absorption spectrum. We note that the spectrum is related through moment theory to the radius of gyration distribution ⁶⁷ and thus its description is improved in the optimization procedure. Its temperature dependence, however, was not part of the optimization and thus provides an important test. The spectrum peak maximum, E_{max} has been found experimentally to redshift with increasing temperature, characterized by the derivative $dE_{max}/dT = -2.2 \times$ 10^{-3} eV/K. $^{67-69}$ This behavior has been challenging for one-electron pseudopotentials to reproduce with the TB and TBOpt models yielding values of dE_{max}/dT that are significantly too small in magnitude, $(-1.9 \pm 0.6) \times 10^{-4}$ and $(-4.4 \pm 0.5) \times 10^{-4}$ eV/K, respectively, ²⁵ and the non-cavity LGS description giving one that is too large, -5.2×10^{-3} eV/K.³³ Thus it is of particular interest for the present empirically optimized pseudopotential.

The absorption spectrum can be obtained in the limit of inhomogeneous broadening as,

$$I(\omega) = \sum_{n=1}^{N_{st}} \langle |\mu_{0n}|^2 \, \delta(\hbar\omega - E_{0n}) \rangle, \qquad (18)$$

where $\mu_{0n} = \langle n|\hat{\mu}|0\rangle$ is the transition dipole moment between the ground state and the n^{th} excited state of the hydrated electron, $E_{0n} =$ $E_n - E_0$ is the corresponding energy difference, and ω is the photon frequency. The contributions from the N_{st} individual transitions are summed to get the total absorption spectrum $I(\omega)$. The first three transitions are dominant,

and the higher energy state transitions contribute mainly to the Lorentzian tail in the blue region; here, we only consider the former so the blue tail does not appear in our spectra. The simulated spectra at four different temperatures are shown in Fig. 8a. We see a clear redshifting of the spectrum as temperature increases in qualitative agreement with experiments. ^{67,69} The key question, however, is whether the empirical optimization procedure has improved the magnitude of the redshift compared to the original TBOpt pseudopotential. This is examined in Fig. 8b where E_{max} is plotted versus T and the slope is determined from a linear fit. We find that the EOP23 pseudopential gives a slope of $dE_{max}/dT = -7.3 \times 10^{-4} \text{ eV/K}$, which is still a factor of three smaller than the experimental value but nearly twice as large as the TBOpt result.

4 Conclusions

We have presented a proof-of-concept optimization of the one electron-water pseudopotential for the hydrated electron to match empirical data. Specifically, we used the measured average radius of gyration and vertical detachment energy to determine the best potential parameters using the TBOpt model as a starting point. The optimization is adequately converged in only 4-5 iterations, yielding good agreement with the target properties.

The optimized pseudopotential differs from the original TBOpt model in two key ways. First, it has a stronger attraction to the water molecule through the polarization potential. Indeed, we find that this term is critical to the optimization as we were unable to converge an optimization using the TB pseudopotential as a starting point, with the only relevant difference being the value used for the water polarizability. Second, the optimized pseudopotential exhibits a weaker attraction of the electron for the water hydrogen atoms.

These changes give the hydrated electron described by the optimized pseudopotential characteristics that are in better accord with available measurements. These were investigated by

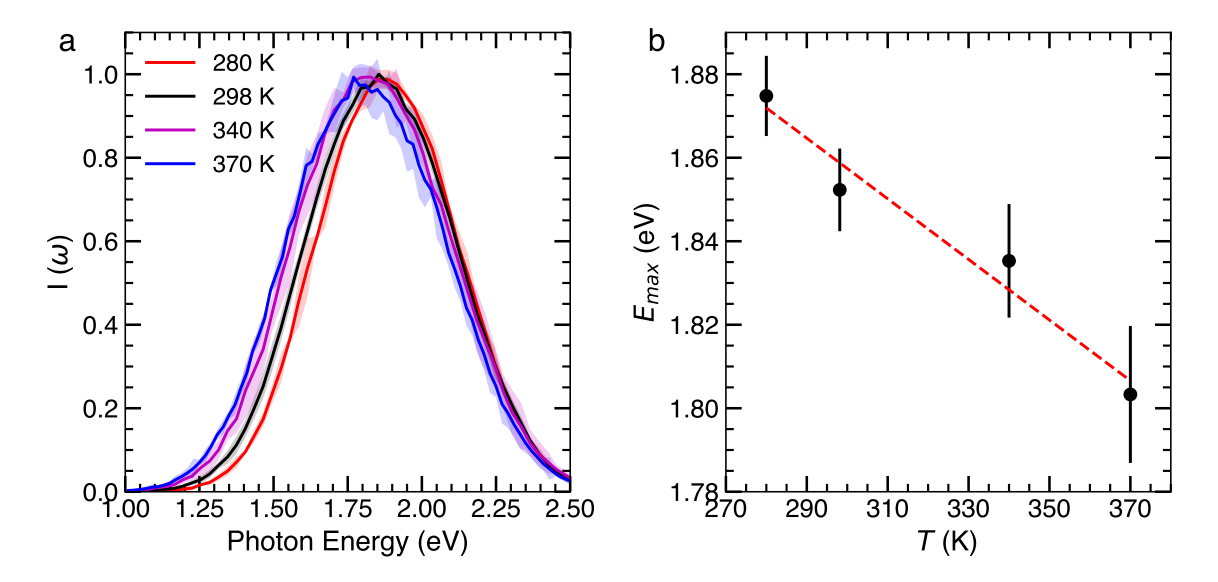


Figure 8: a) The hydrated electron optical spectrum for the EOP23 pseudopotential is plotted for four different temperatures. The shaded regions indicate 95% confidence limits. b) The peak maximum, E_{max} is plotted as a function of temperature (black circles with error bars) along with a linear fit (red dashed line).

constant pressure and temperature simulations. The properties that were explicitly optimized, the radius of gyration and vertical detachment energy, are distinctly improved compared to the original TBOpt pseudopotential. In addition, properties that were not included in the optimization procedure were also shifted toward experimental values. The electron-water radial distribution function adopts a structure that is more similar to that of the TB pseudopotential, with a key change being minima that fall below one. This is a change in the direction of ab initio calculations of the radial distribution function and results in a larger partial molar volume, which is more consistent with the measured value. In addition, the optimized pseudopotential shows a stronger temperature dependence in the radius of gyration and the optical absorption spectrum peak position compared to TBOpt. The weak temperature dependence of these properties has been a key criticism of both the TB and TBOpt models. While the optimized pseudopotential does not result in perfect agreement with the measured values, the improvement in this proof-of-concept study indicates this approach should be a useful route to accurate one-electron descriptions of the hydrated electron.

The present work motivates future attempts to determine empirically optimized hydrated electron pseudopotentials. The work suggests that improvement may be achieved simply through including the water polarizability, α_w , as one of the potential parameters. Additionally, the process can be carried out with an Ewald sum to better represent long-range electrostatic interactions and through simulations at constant pressure to mimic experimental conditions. However, the process is also ultimately limited by the functional form and more flexible alternatives may be required to obtain the best agreement with the hydrated electron measured properties.

Acknowledgments

This work was funded by the Division of Chemical Sciences, Geosciences, and Biosciences, Office of Basic Energy Sciences of the U.S. Department of Energy, through Grant No. DE-SC0021114 (W.H.T.). D.M.B. is supported by the U.S. Department of Energy Office of Science, Office of Basic Energy Sciences under Award Number DE-FC02-04ER1553. The calculations were performed at the University of Kansas Center for Research Computing (CRC),

including including the BigJay cluster resource funded through NSF Grant MRI-2117449.

Supporting Information

Densities of NpT simulations, effects of Ewald sum on the EOP23 hydrated electron properties, temperature dependent RDFs.

References

- (1) Hart, E. J.; Anbar, M. *The Hydrated Electron*; Wiley-Interscience, 1970.
- (2) Buxton, G. V. Radiation chemistry of the liquid state: (1) Water and homogeneous liquid solutions. In *Radiation Chemistry*. *Principles and Applications*; Farhataziz, Rodgers, M. A. J., Eds.; VCH Publishers, 1987.
- (3) Spinks, J. W. T.; Wood, R. J. An Introduction to Radiation Chemistry,; Wiley-Interscience, 1990.
- (4) Garrett, B. C.; Dixon, D. A.; Camaioni, D. M.; Chipman, D. M.; Johnson, M. A.; Jonah, C. D.; Kimmel, G. A.; Miller, J. H.; Rescigno, T. N.; Rossky, P. J. et al. Role of water in electron-initiated processes and radical chemistry: Issues and scientific advances. Chem. Rev. 2005, 105, 355–389.
- (5) Wishart, J., Rao, B., Eds. Recent Trends in Radiation Chemistry,; World Scientific, 2010.
- (6) Kee, T. W.; Son, D. H.; Kambhampati, P.; Barbara, P. F. A unified electron transfer model for the different precursors and excited states of the hydrated electron. J. Phys. Chem. A 2001, 105, 8434–8439.
- (7) Marsalek, O.; Elles, C. G.; Pieniazek, P. A.; Pluhaov, E.; Vandevondele, J.; Bradforth, S. E.; Jungwirth, P. Chasing charge localization and chemical reactivity following photoionization in liquid water. J. Chem. Phys. **2011**, 135.

- (8) Elg, D. T.; Delgado, H. E.; Martin, D. C.; Sankaran, R. M.; Rumbach, P.; Bartels, D. M.; Go, D. B. Recent advances in understanding the role of solvated electrons at the plasma-liquid interface of solution-based gas discharges. Spectrochim. Acta B 2021, 186, 106307.
- (9) Herbert, J. M.; Coons, M. P. The hydrated electron. Annu. Rev. Phys. Chem 2017, 68, 447–472.
- (10) Turi, L.; Rossky, P. J. Theoretical studies of spectroscopy and dynamics of hydrated electrons. *Chem. Rev.* **2012**, *112*, 5641–5674.
- (11) Schnitker, J.; Rossky, P. J. An electronwater pseudopotential for condensed phase simulation. J. Chem. Phys. **1987**, 86, 3462–3470.
- (12) Turi, L.; Borgis, D. Analytical investigations of an electron-water molecule pseudopotential. II. Development of a new pair potential and molecular dynamics simulations. J. Chem. Phys. 2002, 117, 6186–6195.
- (13) Larsen, R. E.; Glover, W. J.; Schwartz, B. J. Does the hydrated electron occupy a cavity? *Science* **2010**, 329, 65–69.
- (14) Jacobson, L. D.; Herbert, J. M. A oneelectron model for the aqueous electron that includes many-body electron-water polarization: Bulk equilibrium structure, vertical electron binding energy, and optical absorption spectrum. *J. Chem. Phys.* **2010**, 133, 154506.
- (15) Uhlig, F.; Marsalek, O.; Jungwirth, P. Unraveling the complex nature of the hydrated electron. *J. Phys. Chem. Lett.* **2012**, *3*, 3071–3075.
- (16) Ambrosio, F.; Miceli, G.; Pasquarello, A. Electronic levels of excess electrons in liquid water. *J. Phys. Chem. Lett.* **2017**, *8*, 2055–2059.

- (17) Pizzochero, M.; Ambrosio, F.; Pasquarello, A. Picture of the wet electron: A localized transient state in liquid water. *Chem. Sci.* **2019**, *10*, 7442–7448.
- (18) Lan, J.; Kapil, V.; Gasparotto, P.; Ceriotti, M.; Iannuzzi, M.; Rybkin, V. V. Simulating the ghost: quantum dynamics of the solvated electron. *Nat. Commun.* **2021**, *12*, 10–15.
- (19) Park, S. J.; Schwartz, B. J. Understanding the temperature dependence and finite size effects in ab initio MD simulations of the hydrated electron. *J. Chem. Theory Comput.* **2022**, *18*, 4973–4982.
- (20) Neupane, P.; Katiyar, A.; Bartels, D. M.; Thompson, W. H. Investigation of the failure of Marcus theory for hydrated electron reactions. *J. Phys. Chem. Lett.* **2022**, *13*, 8971–8977.
- (21) Jonah, C. D.; Romero, C.; Rahman, A. Hydrated electron revisited via the Feynman path integral route. *Chem. Phys. Lett.* **1986**, *123*, 209–214.
- (22) Wallqvist, A.; Thirumalai, D.; Berne, B. J. Path integral Monte Carlo study of the hydrated electron. *J. Chem. Phys.* **1987**, *86*, 6404–6418.
- (23) Sprik, M.; Impey, R. W.; Klein, M. L. Study of electron solvation in polar solvents using path integral calculations. *J. Stat. Phys.* **1986**, *43*, 967–972.
- (24) Larsen, R. E.; Glover, W. J.; Schwartz, B. J. Comment on "An electron-water pseudopotential for condensed phase simulation" [J. Chem. Phys. 86, 3462 (1987)]. J. Chem. Phys. 2009, 131, 37101.
- (25) Glover, W. J.; Schwartz, B. J. Short-range electron correlation stabilizes noncavity solvation of the hydrated electron. *J. Chem. Theory Comput.* **2016**, *12*, 5117–5131.

- (26) Schnitker, J.; Rossky, P. J. Quantum simulation study of the hydrated electron. *J. Chem. Phys.* **1987**, *86*, 3471–3485.
- (27) Wallqvist, A.; Martyna, G.; Berne, B. J. Behavior of the hydrated electron at different temperatures: Structure and absorption spectrum. J. Phys. Chem. 1988, 92, 1721–1730.
- (28) Schwartz, B. J.; Rossky, P. J. Aqueous solvation dynamics with a quantum mechanical solute: Computer simulation studies of the photoexcited hydrated electron. *J. Chem. Phys.* **1994**, *101*, 6902–6916.
- (29) Nicolas, C.; Boutin, A.; Lévy, B.; Borgis, D. Molecular simulation of a hydrated electron at different thermodynamic state points. J. Chem. Phys. 2003, 118, 9689–9696.
- (30) Wilhelm, J.; VandeVondele, J.; Rybkin, V. V. Dynamics of the bulk hydrated electron from many-body wavefunction theory. Angew. Chemie Int. Ed. 2019, 58, 3890–3893.
- (31) Holden, Z. C.; Rana, B.; Herbert, J. M. Analytic gradient for the QM/MM-Ewald method using charges derived from the electrostatic potential: Theory, implementation, and application to ab initio molecular dynamics simulation of the aqueous electron. J. Chem. Phys. 2019, 150, 144115.
- (32) Carter-Fenk, K.; Johnson, B. A.; Herbert, J. M.; Schenter, G. K.; Mundy, C. J. Birth of the hydrated electron via charge-transfer-to-solvent excitation of aqueous iodide. J. Phys. Chem. Lett. 2023, 14, 870–878.
- (33) Casey, J. R.; Kahros, A.; Schwartz, B. J. To be or not to be in a cavity: The hydrated electron dilemma. *J. Phys. Chem. B* **2013**, *117*, 14173–14182.
- (34) Casey, J. R.; Larsen, R. E.; Schwartz, B. J. Resonance Raman and temperaturedependent electronic absorption spectra

- of cavity and noncavity models of the hydrated electron. *Proc. Natl. Acad. Sci. U. S. A.* **2013**, *110*, 2712–2717.
- (35) Zho, C. C.; Schwartz, B. J. Time-resolved photoelectron spectroscopy of the hydrated electron: Comparing cavity and noncavity models to experiment. *J. Phys. Chem. B* **2016**, *120*, 12604–12614.
- (36) Zho, C. C.; Farr, E. P.; Glover, W. J.; Schwartz, B. J. Temperature dependence of the hydrated electron's excited-state relaxation. I. Simulation predictions of resonance Raman and pump-probe transient absorption spectra of cavity and noncavity models. J. Chem. Phys. 2017, 147, 074503.
- (37) Farr, E. P.; Zho, C. C.; Challa, J. R.; Schwartz, B. J. Temperature dependence of the hydrated electron's excited-state relaxation. II. Elucidating the relaxation mechanism through ultrafast transient absorption and stimulated emission spectroscopy. J. Chem. Phys. 2017, 147, 074504.
- (38) Park, S. J.; Schwartz, B. J. Evaluating simple ab initio models of the hydrated electron: The role of dynamical fluctuations. J. Phys. Chem. B **2020**, 124, 9592–9603.
- (39) Glover, W. J.; Schwartz, B. J. The fluxional nature of the hydrated electron: Energy and entropy contributions to aqueous electron free energies. *J. Chem. Theory Comput.* **2020**, *16*, 1263–1270.
- (40) Herbert, J. M.; Jacobson, L. D. Structure of the aqueous electron: Assessment of one-electron pseudopotential models in comparison to experimental data and time-dependent density functional theory. *J. Phys. Chem. A* **2011**, *115*, 14470–14483.
- (41) Neupane, P.; Bartels, D. M.; Thompson, W. H. Partial molar volume of the

- hydrated electron from molecular dynamics simulations. J. Phys. Chem. C 2023, 127, 5941–5947.
- (42) Turi, L.; Madarász, Á. Comment on "Does the hydrated electron occupy a cavity?". *Science* **2011**, *331*, 2010–2012.
- (43) Turi, L. Hydrated electrons in water clusters: Inside or outside, cavity or noncavity? *J. Chem. Theory Comput.* **2015**, *11*, 1745–1755.
- (44) Herbert, J. M. Structure of the aqueous electron. *Phys. Chem. Chem. Phys.* **2019**, 21, 20538–20565.
- (45) Janik, I.; Lisovskaya, A.; Bartels, D. M. Partial molar volume of the hydrated electron. *J. Phys. Chem. Lett.* **2019**, *10*, 2220–2226.
- (46) Lan, J.; Rybkin, V. V.; Pasquarello, A. Temperature dependent properties of the aqueous electron. *Angew. Chem. Int. Ed.* **2022**, e202209398.
- (47) Turi, L. On the applicability of one- and many-electron quantum chemistry models for hydrated electron clusters. J. Chem. Phys. 2016, 144, 154311.
- (48) Luckhaus, D.; Yamamoto, Y.-I.; Suzuki, T.; Signorell, R. Genuine binding energy of the hydrated electron. *Sci. Adv.* **2017**, *3*, e1603224.
- (49) Nishitani, J.; Yamamoto, Y.-i.; West, C. W.; Karashima, S.; Suzuki, T. Binding energy of solvated electrons and retrieval of true UV photoelectron spectra of liquids. Sci. Adv. 2019, 5, eaaw6896.
- (50) Yamamoto, Y.-i.; Suzuki, T. Distortion Correction of Low-Energy Photoelectron Spectra of Liquids Using Spectroscopic Data for Solvated Electrons. J. Phys. Chem. A 2023, 127, 2440-2452.
- (51) Golden, S.; Tuttle, T. R. Nature of solvated electron absorption spectra. *J. Chem. Soc. Faraday Trans. 2 Mol. Chem. Phys.* **1979**, 75, 474–484.

- (52) Tuttle, T. R.; Golden, S. Solvated electrons: What is solvated? *J. Phys. Chem.* **1991**, *95*, 5725–5736.
- (53) Feynman, R. P. Forces in molecules. *Phys. Rev.* **1939**, *56*, 340–343.
- (54) Aizu, K. Parameter Differentiation of Quantum-Mechanical Linear Operators. J. Math. Phys. 1963, 4, 762–775.
- (55) Wu, Y.; Tepper, H. L.; Voth, G. A. Flexible simple point-charge water model with improved liquid-state properties. *J. Chem. Phys.* **2006**, *124*, 024503.
- (56) Toukan, K.; Rahman, A. Molecular-dynamics study of atomic motions in water. *Phys. Rev. B* **1985**, *31*, 2643–2648.
- (57) Bussi, G.; Donadio, D.; Parrinello, M. Canonical sampling through velocity rescaling. *J. Chem. Phys.* **2007**, *126*, 014101.
- (58) Colbert, D. T.; Miller, W. H. A novel discrete variable representation for quantum mechanical reactive scattering via the S-matrix Kohn method. J. Chem. Phys. 1992, 96, 1982–1991.
- (59) Bernetti, M.; Bussi, G. Pressure control using stochastic cell rescaling. *J. Chem. Phys.* **2020**, *153*, 114107.
- (60) Shoemaker, D. P.; Garland, C. W.; Nibler, J. W. Experiments in Physical Chemistry; McGraw-Hill: New York, 1989.
- (61) Kirkwood, J. G.; Buff, F. P. The statistical mechanical theory of solutions. I. J. Chem. Phys. 1951, 19, 774–777.
- (62) Ben-Naim, A. The Kirkwood–Buff integrals for one-component liquids. *J. Chem. Phys.* **2008**, *128*, 234501.
- (63) Dawass, N.; Krüger, P.; Schnell, S. K.; Simon, J.-M.; Vlugt, T. J. H. Kirkwood-Buff integrals from molecular simulation. *Fluid Ph. Equilibria* **2019**, *486*, 21–36.

- (64) Krüger, P.; Vlugt, T. J. H. Size and shape dependence of finite-volume Kirkwood-Buff integrals. *Phys. Rev. E* **2018**, *97*, 051301.
- (65) Primorac, T.; Požar, M.; Sokolić, F.; Zoranić, L. The influence of binary mixtures' structuring on the calculation of Kirkwood-Buff integrals: A molecular dynamics study. J. Mol. Liq. 2021, 324, 114773.
- (66) Borsarelli, C. D.; Bertolotti, S. G.; Previtali, C. M. Thermodynamic changes associated with the formation of the hydrated electron after photoionization of inorganic anions: A time-resolved photoacoustic study. *Photochem. Photobiol. Sci.* 2003, 2, 791–795.
- (67) Bartels, D. M.; Takahashi, K.; Cline, J. A.; Marin, T. W.; Jonah, C. D. Pulse radiolysis of supercritical water. 3. Spectrum and thermodynamics of the hydrated electron. J. Phys. Chem. A 2005, 109, 1299–1307.
- (68) Jou, F.-Y.; Freeman, G. R. Temperature and isotope effects on the shape of the optical absorption spectrum of solvated electrons in water. *J. Phys. Chem.* **1979**, *83*, 2383–2387.
- (69) Du, Y.; Price, E.; Bartels, D. M. Solvated electron spectrum in supercooled water and ice. *Chem. Phys. Lett.* **2007**, *438*, 234–237.

Graphical TOC Entry

